Supporting Information for

Molecular Characterization of Composition and Volatility of Ambient Organic Aerosol Sampled by an UAV-mounted Portable Aethalometer

*Qiaorong Xie,[1] Eli Windwer,[4] Isaac S. Morton,[3] Kelsey E. Lavin,[1] Emily R. Halpern,[1] Dori Nissenbaum,[4] Sergey A. Nizkorodov,[5] Yinon Rudich,[4] Alexander Laskin[1,2]**

[1] *Department of Chemistry, Purdue University, West Lafayette, Indiana, 47907, United States*

[2] *Department of Earth, Atmospheric, and Planetary Sciences, Purdue University, West Lafayette, Indiana, 47907, United States*

[3]*Davidson School of Chemical Engineering, Purdue University, West Lafayette, Indiana, 47907, United States*

[4]*Department of Earth and Planetary Sciences, Weizmann Institute of Science, Rehovot 76100, Israel*

[5]*Department of Chemistry, University of California, Irvine, Irvine, California 92697, United States*

**Corresponding author: alaskin@purdue.edu*

Table of Contents

Supplemental Note 1. Filed Deployment and Real-time Measurements.

Black and Brown Carbon concentrations and absorption coefficients. Atmospheric mass loadings and absorption coefficients of black carbon (BC) and brown carbon (BrC) were determined using the MA200 micro-aethalometer, which continuously collects ambient aerosol particles onto a Teflon filter tape at a flow rate of 0.1 L min^{-1}. Particles larger than 2.5 µm are removed by a microCyclone™ $PM_{2.5}$ cyclonic separator before deposition. Aerosol deposition occurs at a specific spot on the tape, where light absorption is measured at five distinct wavelengths using photomultiplier tubes (PMTs). In 'DualSpot' operational mode, two distinct regions of the filter tape are simultaneously exposed to aerosol flows at different face velocities, allowing for real-time correction of uneven particle loading. The mass concentration of light-absorbing carbon (LAC), expressed as BC-equivalent, is calculated via Equation S1:

$$C_{\mathrm{BCeq},\lambda}^{\mathrm{mass}} = f \frac{\alpha_{\mathrm{abs},\lambda}}{\sigma_{\mathrm{ATN},\lambda}(\mathrm{MA200})} \quad \text{(S1)}$$

where, $C_{\mathrm{BCeq},\lambda}^{\mathrm{mass}}$ is the equivalent black carbon mass concentration in units of $\mathrm{g\,m^{-3}}$ at wavelength λ; $\alpha_{\mathrm{abs},\lambda}$ is the absorption coefficient of LAC at wavelength λ in units of $\mathrm{Mm^{-1}}$; $\sigma_{\mathrm{ATN},\lambda}(\mathrm{MA200})$ is the specific attenuation cross-section in units of $\mathrm{m^2\,g^{-1}}$, provided for the MA200 by the manufacturer (Table S1); f is a multiple scattering coefficient, empirically calculated as 1.3 for the MA200 when running the dual-spot correction mode, compensating for the filter's effect.

Table S1. The table shows MA200 instrument-specific MAE (mass absorption efficiency) values for each wavelength, as given by the MA200's manufacturer.

Wavelength name	Wavelength [nm]	MAE [$\mathrm{m^2\,g^{-1}}$]
UV	375	24.069
Blue	470	19.070
Green	528	17.070
Red	625	14.091
IR	880	10.120

Measurements at 880 nm are interpreted as presenting BC concentrations, while measurements at other wavelengths capture contributions from both BC and BrC. The absorption contributions

of BC and BrC were deconvoluted using the approach described by Li *et al.*[1]. Absorption coefficients were calculated using Equation S2.

$$\alpha_{\text{abs},\lambda} = \frac{C_{\text{BC},\lambda}^{\text{mass}} \cdot \sigma_{\text{ATN},\lambda}(\text{MA200})}{f} \quad \text{(S2)}$$

The total LAC absorption coefficients were fitted to the power law based on Equation S3:

$$\alpha_{\text{abs},\lambda} = \alpha_0 \lambda^{-AAE} \quad \text{(S3)}$$

where AAE is the Absorption Ångström Exponent (unitless) and α_0 is a specific coefficient in units of Mm^{-1}. AAE represents the spectral dependence of LACs in the sample.[2] The fit produced the following relations: $\alpha_{abs}^{15m}(\lambda) = 2.99 \cdot 10^6 \cdot \lambda^{-1.50}$ (RMSE = 2.11) and $\alpha_{abs}^{200m}(\lambda) = 2.34 \cdot 10^5 \cdot \lambda^{-1.22}$ (RMSE = 2.41) for 15 and 200 m altitudes, respectively.

BC is characterized by AAE=1.[3, 4] However, for the MA200 micro-aethalometer, a corrected AAE value of 1.02 has been established for BC. Absorption at longer wavelengths (e.g., 880 nm) is attributed exclusively to BC, as the contribution of BrC at these wavelengths is considered negligible.[5, 6] Consequently, the absorption contribution of BC across the 375–625 nm range can be determined using by Equation S4: Consequently, the absorption contribution of BC across the 375–625 nm range can be determined using Equation S4.

$$\frac{\alpha_{\text{BC},\lambda}}{\alpha_{\text{abs},880}} = \left(\frac{\lambda}{880}\right)^{-1.02} \quad \text{(S4)}$$

where $\alpha_{\text{BC},\lambda}$ is the absorption coefficient attributed to BC only.

The difference between the total LAC absorption and the BC absorption is attributed to BrC, as defined by Equation S5:

$$\alpha_{\text{BrC},\lambda} = \alpha_{\text{abs},\lambda} - \alpha_{\text{BC},\lambda} \quad \text{(S5)}$$

where, AAE values for BC and BrC are determined by fitting the obtained $\alpha_{\text{BrC},\lambda}$ and $\alpha_{\text{BC},\lambda}$ data. The relationships for BC absorption at 15 m and 200 m altitudes are given by: $\alpha_{BC}^{15m}(\lambda) = 1.20 \cdot 10^5 \cdot \lambda^{-1.02}$ and $\alpha_{BC}^{200m}(\lambda) = 5.57 \cdot 10^4 \cdot \lambda^{-1.02}$. These fits exhibit an RMSE of 0, consistent with the assumption that BC absorption follows an AAE of 1.02, as defined by Equation S4. For BrC, the best-fit absorption relationships are: $\alpha_{BrC}^{15m}(\lambda) = 2.73 \cdot 10^{10} \cdot \lambda^{-3.23}$ (RMSE = 4.46) and $\alpha_{BrC}^{200m}(\lambda) = 1.17 \cdot 10^7 \cdot \lambda^{-2.15}$ (RMSE = 3.14). These results highlight the distinct spectral dependencies of BrC absorption at the two altitudes. The complete code used for fitting and analysis is available at https://doi.org/10.5281/zenodo.15475227.

Mass concentration analysis. The OPC-N3 is a compact Optical Particle Counter that measures particle size distributions in real-time. Ambient air is drawn into the optical chamber, where particles scatter light from a 5–8 mW laser operating at a wavelength of 658 nm. This light scattering is used to determine particle diameters at a rate of up to 10,000 particles per second. The onboard electronics classify the measured particle sizes into 24 bins, covering a size range 0.35 to 40 μm.

Binned particle number size distributions (PNSD) were measured by the OPC-N3 at each altitude. The raw binned data has been processed using the standard $dN/d(\log D_p)$ format and averaged over the flight duration at each designated altitude after signal stabilization. Mass concentrations were directly obtained from the OPC-N3, with PM_1, $PM_{2.5}$, and PM_{10} values calculated using an assumed particle density of 1.59 g cm^{-3}.

Mass absorption coefficient calculation. The mass absorption coefficient of OA at a specific wavelength (λ), denoted as $MAC_{OA,\lambda}$, is calculated using the absorption coefficient ($\alpha_{BrC,\lambda}$) and the mass concentration of OA (M_{OA}):

$$MAC_{OA,\lambda} = \alpha_{BrC,\lambda}/M_{OA} \quad \text{(S6).}$$

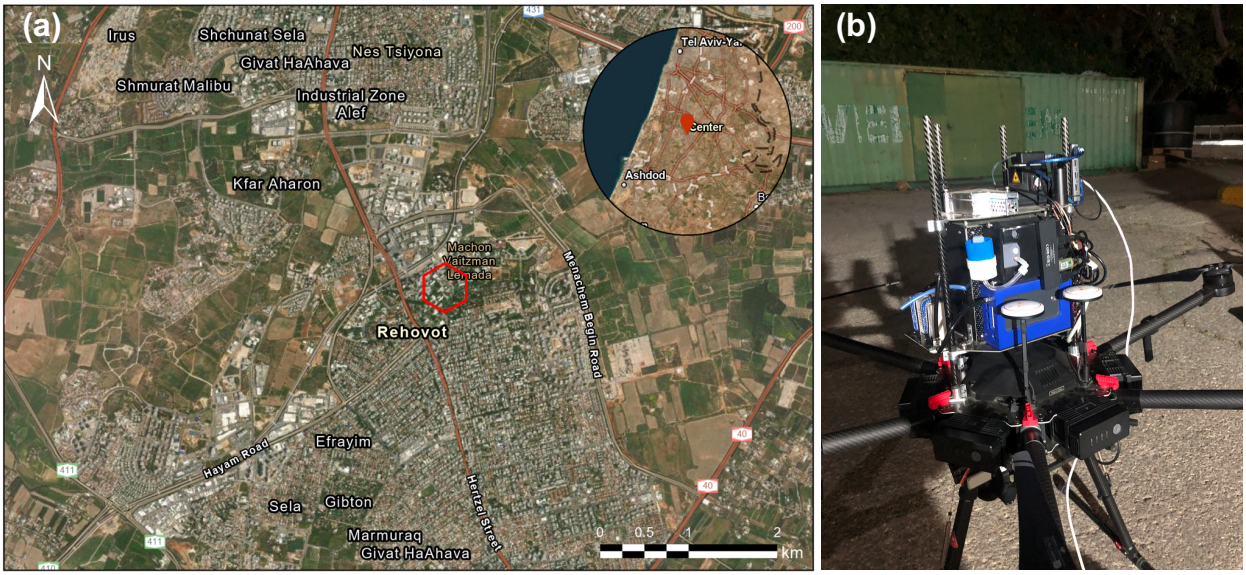

Figure S1. Sampling location and an unmanned aerial vehicle (UAV) platform used for aerosol measurements. (a) A satellite image of the Weizmann Institute of Science (WIS) campus. The red octagon marks the UAV flight range location, at the center of the campus. The inset map shows WIS in relation to major Israel cities and the Mediterranean Sea. The map was produced by ESRI/ArcGIS. The WIS campus features low-rise buildings and is bordered by the city of Rehovot to the south and a High-Tech industrial area to the north, which is comprised mostly of office buildings. A train station is situated between the campus and the High-Tech park. Open agricultural fields lie to the east and west, with the Mediterranean Sea 12 km to the west. (b) Configuration of the UAV during the experiment. The MA200 UAV is mounted in a blue chassis. A black inlet tube connects the micro-cyclone and dryer unit. The optical particle counter (OPC-N3) is positioned at the top of the assembly.

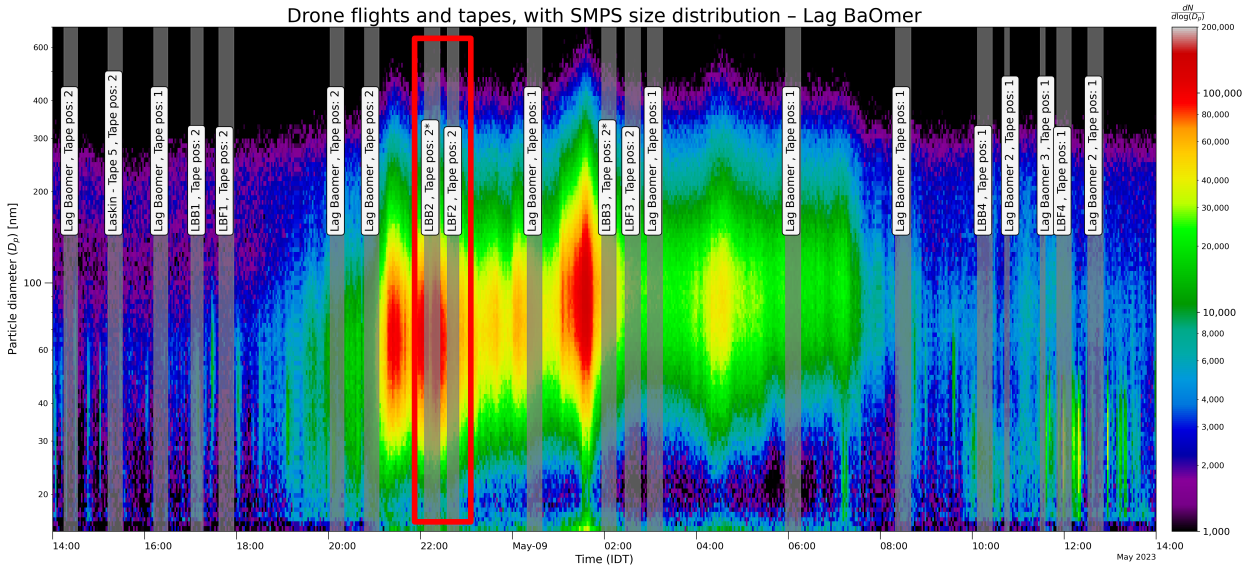

Figure S2. The particle number size distribution measured during Lag Ba'Omer event with a Scanning Mobility Particle Sizer (SMPS) located at the ground. The red frame is the Lag Ba'Omer event period, and the samples (LBB2 and LBF2 at flight altitudes of 15 m and 200 m) collected during this period are selected as the case samples for TPD-DART- HRMS characterization.

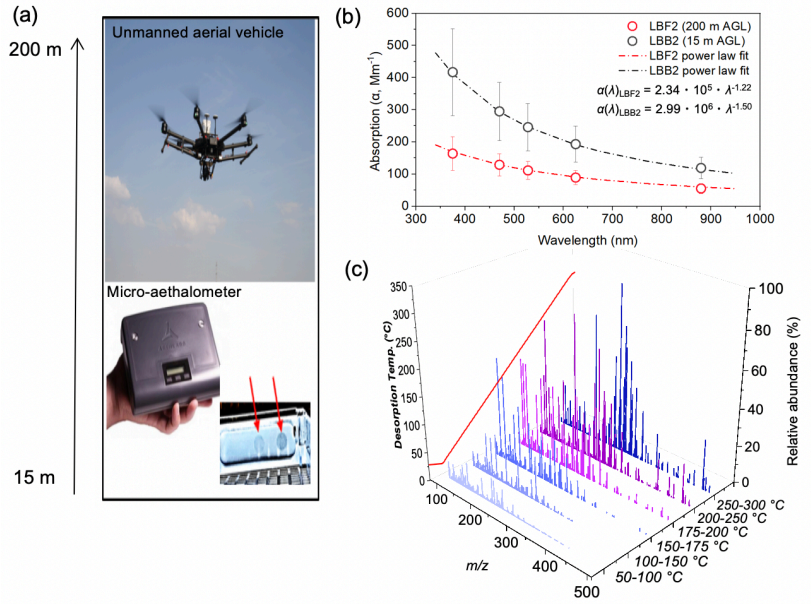

Figure S3. UAV-based sampling and analysis of organic aerosol. (a) UAV was equipped a micro-aethalometer to collect the OA samples at altitudes of 15 m and 200 m. (b) Light absorption data obtained from micro-aethalometer. (c) Progression of (−)DART-HRMS spectra of an OA sample collected by micro-aethalometer, averaged over the annotated temperature intervals of the TPD experiment. The thermal desorption temperature profile (red line) is overlaid on the secondary *y*-axis.

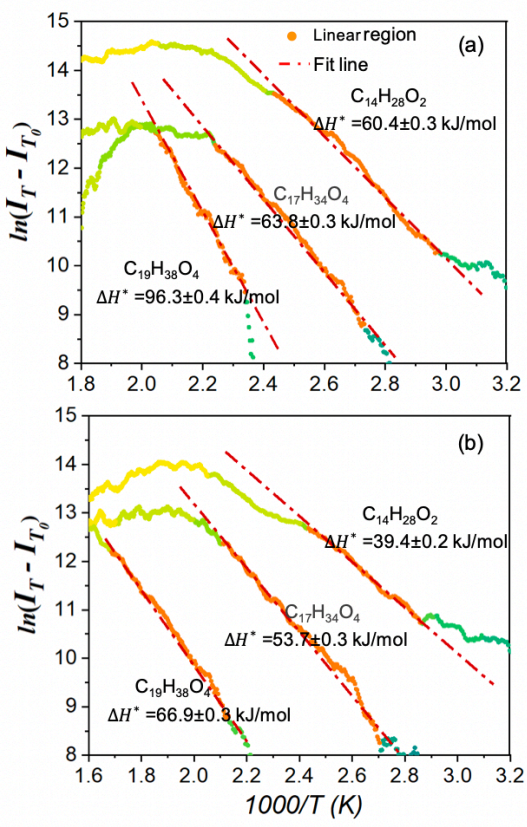

Figure S4. Arrhenius plots of $ln(I_T - I_{T0})$ versus $1/T$ (K^{-1}) of three selected species of $C_{14}H_{28}O_2$, $C_{17}H_{34}O_4$, and $C_{18}H_{36}O_3$ in the aerosol samples collected at (a) 200 m and (b) 15 m. Orange symbols denote linear regions used to fit (red dashed lines) the data using Clausius−Clapeyron equation and calculate the apparent enthalpies of solid-to-gas transitions, shown in legends. The color scale reflects viscosity values calculated for each species as a function of temperature during the TPD run.

Supplemental Note 2. Construction of VBS distributions.

The VBS framework, a method that segments the volatility spectrum of OA components into distinct bins,[7, 8] is utilized to describe the entire range of saturation vapor pressures within the system. Based on their C^*_T values, individual species (i) are grouped into a series of bins (j), defined by integer values of $(\log C^*)_j$. The relative heights ($H_{T,j}$) of VBS bins j are calculated as the sum of the mass fractions of species contained within each bin, normalized to the sum of heights across all bins, expressed by Equation S7:

$$H_{T,j} = \frac{[\sum_i f_i \ {}^{i}C_T^*]_j}{\sum_j [\sum_i f_i \ {}^{i}C_T^*]_j}, \text{ where } \sum_j H_j = 1 \quad \text{(S7)}$$

where f_i is the mass fraction of species i, derived from TPD-HRMS thermogram using Equation S8:

$$f_i = \frac{\sigma_i \times h_i \times MW_i}{\sum_i \ \sigma_i \times h_i \times MW_i} \quad where \ \sum_i f_i = 1 \quad \text{(Eq. 8)}$$

where MW_i is the molecular weight of the detected neutral species (i); h_i represents the integrated area of the single ion thermogram (SIT) corresponding to its characteristic parent ion; σ_i represents a sensitivity factor accounting for the relative ionization efficiency of each species. For the laboratory generated BBOA mixture, our previous study[9] has shown that σ_i values can be approximated to be uniform, allowing them to cancel out in both the numerator and denominator of Equation 8.

The particle-phase mass fractions of aerosolized SOA mixtures for each individual bin j are then computed using the constructed VBS distributions. This calculation takes into account different values of the total organic mass (*tOM)* loadings in the air (e.g., 1, 10, 100 μg m^{-3}) using the following equation (Eq. S9):

$$X_j^P = H_j \times \frac{C_{tOM}}{C_{tOM} + \sum_i \ {}^{i}C_T^*} \quad \text{(S9)}$$

where C_{tOM} is the total organic mass loading; ${}^{i}C_T^*$ is the temperature-dependent saturated mass concentration of component (i) with volatility within bin j.

Supplemental Note 3. Viscosity, diffusion coefficient, and *e*-folding time calculations.

The glass transition temperature ($T_{g,i}$) of each organic component (i) is estimated using a parameterization method based on the number of carbon (n_C), hydrogen (n_H), and oxygen (n_O) atoms in the corresponding elemental formula. The estimation employs Equation S10 shown below along with parameter values for n_C^0, b_C, b_H, b_{CH}, b_O, and b_{CO} listed in previous reports.[10]

$$T_{g,i} = (n_C^o + \ln(n_C))b_C + \ln(n_H)\, b_H + \ln(n_C)\ln(n_H)\, b_{CH} + \ln(n_O)\, b_O + \ln(n_C)\ln(n_O) b_{CO} \quad \text{(S10)}$$

The glass transition temperature ($T_g(\omega_{org})$) of OA mixtures in a form of aerosolized particles containing water is estimated using the Gordon-Taylor equation S11:[10, 11]

$$T_g(\omega_{org}) = \frac{(1-\omega_{org})T_{g,w} + \frac{1}{K_{GT}}\omega_{org}T_{g,org}}{(1-\omega_{org}) + \frac{1}{K_{GT}}\omega_{org}} \quad \text{(S11)}$$

Here, ω_{org} is the organic mass fraction in the OA particles containing water, computed as ω_{org} = mOA /(mOA + mH$_2$O), where mOA and mH$_2$O are particle phase masses of SOA and water, respectively. For each of the environmental conditions of T (K) and tOM (μg·m^{-3}) considered, mOA is calculated by summing the particle-phase mass fractions across all bins j comprising the corresponding VBS distribution. Values of mH$_2$O are subsequently calculated for OA-water aerosol mixtures equilibrated at various RH using the modified Kohler theory,[12] assuming the effective hygroscopicity parameter of κ_{BBOA} = 0.057 ± 0.07.[11, 13] The glass transition temperature ($T_{g,org}$) of the aerosolized OA mixture is calculated as $T_{g,org} = \sum_i \omega_i\, T_{g,i}$, where ω_i represents the mass fraction of each component i present in the VBS-calculated particle phase.[14] The glass transition temperature of pure water ($T_{g,w}$) and the Gordon-Taylor constant (k_{GT}) were set as 136 K and 2.5, respectively.[15]

The viscosity (η, Pa·s) of individual organic components and their mixtures have been calculated from $T_{g,i}$ and $T_{g,org}$, respectively, using the Vogel-Tammann-Fulcher equation (Eq. 12):[10]

$$log\eta = -5 + 0.434\frac{T_0 D}{T_g - T_0} \quad \text{(S12)}$$

where T_0 is the Vogel temperature ($T_0 = 39.17 \times T_g/(D + 39.17)$ and D is the fragility parameter, assumed to be 10 when $T_g < T$.[10] Finally, viscosity values derived for mixtures of interest are used to calculate their corresponding diffusion coefficients (D_b) using the Stokes-Einstein equation S13:

$$D_{\mathrm{b}} = \frac{kT}{6\pi a\eta} \quad \text{(S13)}$$

where k is the Boltzmann constant (1.38×10^{-23} J K^{-1}) and a is the effective molecular radius approximated as 1 nm.[15, 16]

The characteristic *e*-folding times (τ_{mix}, s) for OA mixtures were calculated with the following Equation S14:[17]

$$\tau_{mix} = \frac{{d_p}^2}{4\pi^2 D_b} \quad \text{(S14)}$$

where d_p is the particle diameter.

Supplemental Note 4. Molecular composition of OA from test burns of commercial urban materials.

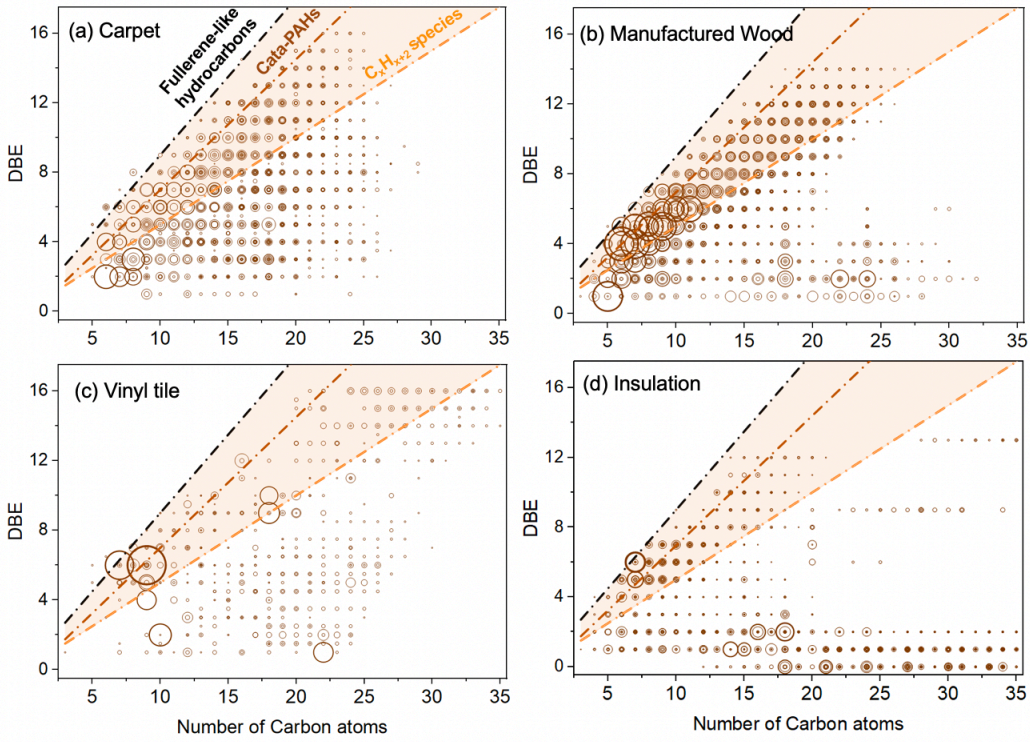

Figure S5. The double bond equivalent (DBE) values vs. number of carbon atoms corresponding to the components of OA samples from thermal dfecomposition of urban materials, i.e., carpet,[18] manufactured wood, insulation, and vinyl tile, detected by TPD-DART-HRMS. Lines indicate DBE reference values of linear conjugated polyenes C_xH_{x+2} (orange line), cata-condensed PAHs (brown line), and fullerene-like hydrocarbons (black line). Data points inside the orange shaded area are potential BrC chromophores.[19] Sizes of the individual points are arbitrarily scaled to the cubic root of the corresponding MS peaks intensities. Occasional datapoints located above the fullerene-like limiting line correspond to highly aromatic N-containing species.

Supplemental Note 5. VBS distributions and gas-particle partitioning of OA mixtures under variable *T* and *tOM* conditions.

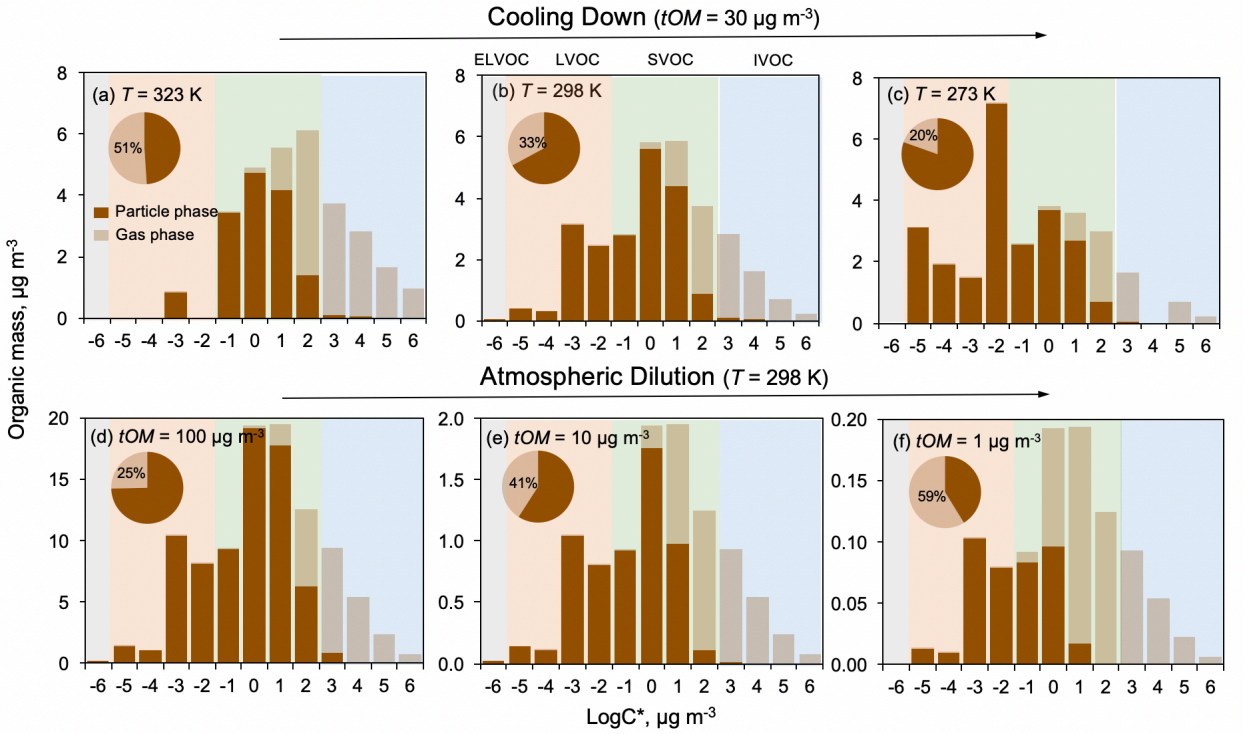

Figure S6. (a-c) Volatility basis set (VBS) distributions for components of 200 m mixtures, calculated at constant mass loading of *tOM* = 30 µg m^{-3} decreasing temperatures (278 K, 288 K, and 298 K); (d-f) at constant *T* = 298K and decreasing total organic mass (*tOM*) loadings (100, 10, and 1 µg m^{-3}). Pie charts indicate the total gas-phase and particle-phase mass fractions.

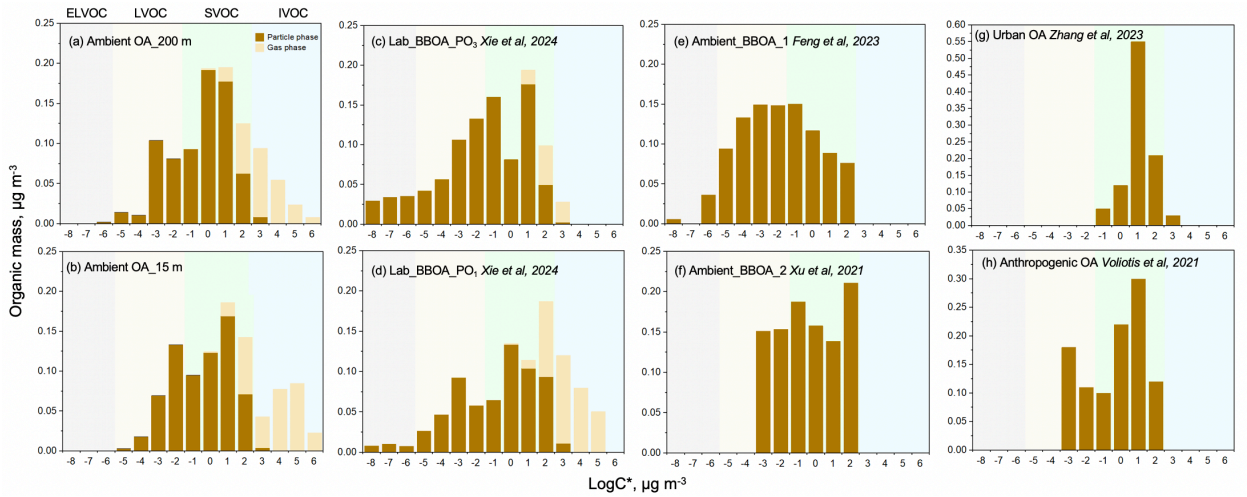

Figure S7. The comparison of VBS distribution for OA components in samples from (a) 200 m and (b) 15 m mixtures, calculated at T= 298 K and tOM=100 μg m^{-3}. Literature values of BBOA_PO_3 (c) and BBOA_PO_1 (d) in lab studies detected by TPD-DART-HRMS[20] and ambient BBOA_1[21] (e) and BBOA_2[22] (f) from field studies detected by aerosol mass spectrometer, as well as the urban OA (g)[23] and anthropogenic (h)[24] OA are shown for comparison. Light and dark colors indicate the gas-phase and particle-phase fractions, respectively.

Supplemental Note 6. Viscosity of OA mixtures as a function of RH and *T*.

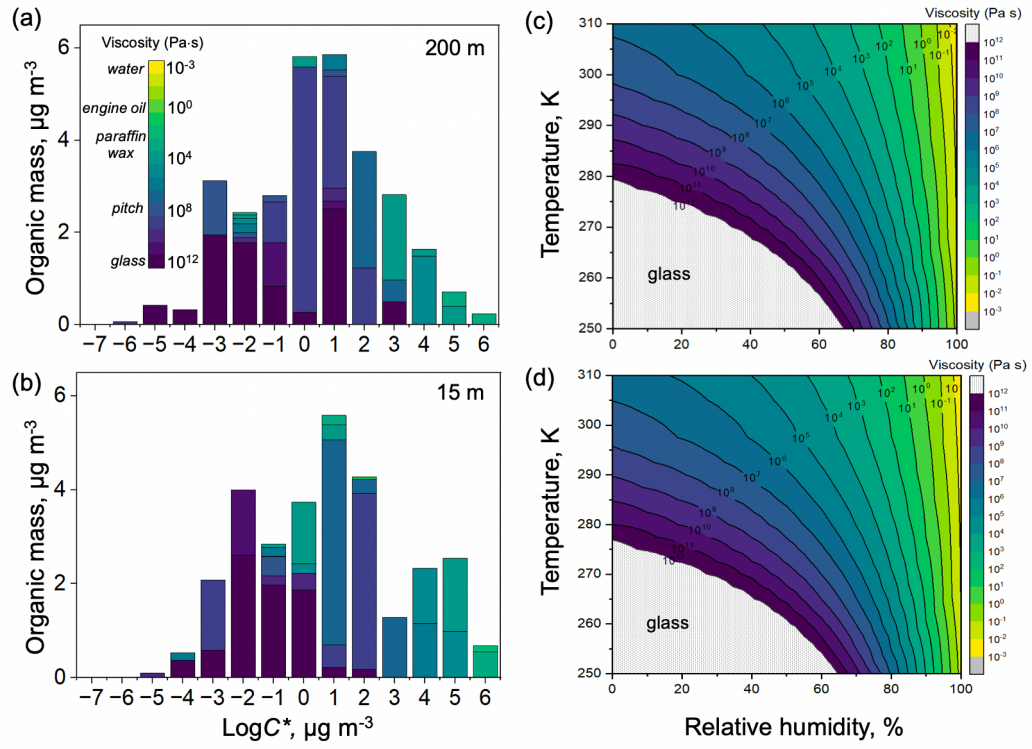

Figure S8. (a, b) The VBS distributions incorporating information on viscosity values calculated for individual components identified in the mixtures at 200 m (a) and 15 m (b) under ambient conditions of T=298 K and tOM=30 μg m^{-3}. Each bin in the VBS distributions is color-coded to represent contributions of components with varying viscosity ranges. (c-d) Viscosity maps of OA mixtures at 200 m (c) and 15 m (d) as a function of T and RH.

References

1. Li, C.; Windwer, E.; Fang, Z.; Nissenbaum, D.; Rudich, Y., Correcting micro-aethalometer absorption measurements for brown carbon aerosol. *Sci. Total Environ.* **2021,** *777*, 146143.
2. Ångström, A., On the atmospheric transmission of sun radiation and on dust in the air. *Geografiska Annaler* **1929,** *11*, (2), 156-166.
3. Zhao, Z.; Cao, J.; Chow, J. C.; Watson, J. G.; Chen, A. L.; Wang, X.; Wang, Q.; Tian, J.; Shen, Z.; Zhu, C., Multi-wavelength light absorption of black and brown carbon at a high-altitude site on the Southeastern margin of the Tibetan Plateau, China. *Atmos. Environ.* **2019,** *212*, 54-64.
4. Zhang, Y.; Albinet, A.; Petit, J.-E.; Jacob, V.; Chevrier, F.; Gille, G.; Pontet, S.; Chrétien, E.; Dominik-Sègue, M.; Levigoureux, G., Substantial brown carbon emissions from wintertime residential wood burning over France. *Sci. Total Environ.* **2020,** *743*, 140752.
5. Kirchstetter, T. W.; Novakov, T.; Hobbs, P. V., Evidence that the spectral dependence of light absorption by aerosols is affected by organic carbon. *J. Geophys. Res.-Atmos.* **2004,** *109*, (D21).
6. Li, S.; Zhu, M.; Yang, W.; Tang, M.; Huang, X.; Yu, Y.; Fang, H.; Yu, X.; Yu, Q.; Fu, X., Filter-based measurement of light absorption by brown carbon in PM2. 5 in a megacity in South China. *Sci. Total Environ.* **2018,** *633*, 1360-1369.
7. Donahue, N. M.; Kroll, J.; Pandis, S. N.; Robinson, A. L., A two-dimensional volatility basis set–Part 2: Diagnostics of organic-aerosol evolution. *Atmos. Chem. Phys.* **2012,** *12*, (2), 615-634.
8. Donahue, N. M.; Epstein, S. A.; Pandis, S. N.; Robinson, A. L., A two-dimensional volatility basis set: 1. organic-aerosol mixing thermodynamics. *Atmos. Chem. Phys.* **2011,** *11*, (7), 3303-3318.
9. Xie, Q.; Gerrebos, N. G. A.; Calderon-Arrieta, D.; Morton, I. S.; Halpern, E. R.; Li, C.; Zeng, M. F.; Bertram, A. K.; Rudich, Y.; Laskin, A., Molecular Insights into Gas–Particle Partitioning and Viscosity of Atmospheric Brown Carbon. *Environ. Sci. Technol.* **2024,** *58*, (41), 18284–18294.
10. DeRieux, W.-S. W.; Li, Y.; Lin, P.; Laskin, J.; Laskin, A.; Bertram, A. K.; Nizkorodov, S. A.;

Shiraiwa, M., Predicting the glass transition temperature and viscosity of secondary organic material using molecular composition. *Atmos. Chem. Phys.* **2018,** *18*, (9), 6331-6351.
11. Galeazzo, T.; Valorso, R.; Li, Y.; Camredon, M.; Aumont, B.; Shiraiwa, M., Estimation of secondary organic aerosol viscosity from explicit modeling of gas-phase oxidation of isoprene and α-pinene. *Atmos. Chem. Phys.* **2021,** *21*, (13), 10199-10213.
12. Petters, M.; Kreidenweis, S., A single parameter representation of hygroscopic growth and cloud condensation nucleus activity. *Atmos. Chem. Phys.* **2007,** *7*, (8), 1961-1971.
13. Bougiatioti, A.; Bezantakos, S.; Stavroulas, I.; Kalivitis, N.; Kokkalis, P.; Biskos, G.; Mihalopoulos, N.; Papayannis, A.; Nenes, A., Biomass-burning impact on CCN number, hygroscopicity and cloud formation during summertime in the eastern Mediterranean. *Atmos. Chem. Phys.* **2016,** *16*, (11), 7389-7409.
14. Dette, H. P.; Qi, M.; Schröder, D. C.; Godt, A.; Koop, T., Glass-forming properties of 3-methylbutane-1, 2, 3-tricarboxylic acid and its mixtures with water and pinonic acid. *J. Phys. Chem. A* **2014,** *118*, (34), 7024-7033.
15. Koop, T.; Bookhold, J.; Shiraiwa, M.; Pöschl, U., Glass transition and phase state of organic compounds: dependency on molecular properties and implications for secondary organic aerosols in the atmosphere. *Phys. Chem. Chem. Phys.* **2011,** *13*, (43), 19238-19255.
16. Evoy, E.; Maclean, A. M.; Rovelli, G.; Li, Y.; Tsimpidi, A. P.; Karydis, V. A.; Kamal, S.; Lelieveld, J.; Shiraiwa, M.; Reid, J. P., Predictions of diffusion rates of large organic molecules in secondary organic aerosols using the Stokes–Einstein and fractional Stokes–Einstein relations. *Atmos. Chem. Phys.* **2019,** *19*, (15), 10073-10085.
17. Seinfeld, J. H.; Pandis, S. N., *Atmospheric chemistry and physics: from air pollution to climate change*. John Wiley & Sons: 2016.
18. Hopstock, K. S.; Klodt, A. L.; Xie, Q.; Alvarado, M. A.; Laskin, A.; Nizkorodov, S. A., Photolytic aging of organic aerosol from pyrolyzed urban materials. *Environ. Sci. Atmos.* **2023,** *3*, (9), 1272-1285.
19. Cain, J.; Laskin, A.; Kholghy, M. R.; Thomson, M. J.; Wang, H., Molecular characterization of organic content of soot along the centerline of a coflow diffusion flame. *Phys. Chem. Chem. Phys.* **2014,** *16*, (47), 25862-25875.

20. Xie, Q.; Gerrebos, N. G. A.; Calderon-Arrieta, D.; Morton, I. S.; Halpern, E. R.; Li, C.; Zeng, M. F.; Bertram, A. K.; Rudich, Y.; Laskin, A., Molecular Insights into Gas–Particle Partitioning and Viscosity of Atmospheric Brown Carbon. *Environ. Sci. Technol.* **2024,** *58*, (41), 18284-18294.
21. Feng, T.; Wang, Y.; Hu, W.; Zhu, M.; Song, W.; Chen, W.; Sang, Y.; Fang, Z.; Deng, W.; Fang, H., Impact of aging on the sources, volatility, and viscosity of organic aerosols in Chinese outflows. *Atmos. Chem. Phys.* **2023,** *23*, (1), 611-636.
22. Xu, W.; Chen, C.; Qiu, Y.; Li, Y.; Zhang, Z.; Karnezi, E.; Pandis, S. N.; Xie, C.; Li, Z.; Sun, J.; Ma, N.; Xu, W.; Fu, P.; Wang, Z.; Zhu, J.; Worsnop, D. R.; Ng, N. L.; Sun, Y., Organic aerosol volatility and viscosity in the North China Plain: contrast between summer and winter. *Atmos. Chem. Phys.* **2021,** *21*, (7), 5463-5476.
23. Zhang, Y.; Huang, H.; Qin, W.; Yu, Q.; Sun, Y.; Cheng, S.; Ahmad, M.; Ouyang, W.; Soyol-Erdene, T.-O.; Chen, J., Modeling of wintertime regional formation of secondary organic aerosols around Beijing: sensitivity analysis and anthropogenic contributions. *Carbon Res.* **2023,** *2*, (1), 6.
24. Voliotis, A.; Wang, Y.; Shao, Y.; Du, M.; Bannan, T. J.; Percival, C. J.; Pandis, S. N.; Alfarra, M. R.; McFiggans, G., Exploring the composition and volatility of secondary organic aerosols in mixed anthropogenic and biogenic precursor systems. *Atmos. Chem. Phys.* **2021,** *21*, (18), 14251-14273.